

DOE Award No.: DE-FE-0009963

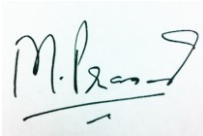
Quarterly Research Performance Progress Report (Period ending 12/31/2015)

Measurement and Interpretation of Seismic Velocities and Attenuations
in Hydrate-Bearing Sediments

Project Period (10/1/2012 to 4/30/2016)

Submitted by:

PI: Manika Prasad
Colorado School of Mines
DUNS #010628170.
1500 Illinois Street
Golden, CO 80401
e-mail: mprasad@mines.edu
Phone number: (303) 273-3457
Submission Date: 1/31/2016



Prepared for:

United States Department of Energy
National Energy Technology Laboratory



Office of Fossil Energy

Disclaimer

This report was prepared as an account of work sponsored by an agency of the United States Government. Neither the United States Government nor any agency thereof, nor any of their employees, makes any warranty, express or implied, or assumes any legal liability or responsibility for the accuracy, completeness, or usefulness of any information, apparatus, product, or process disclosed, or represents that its use would not infringe privately owned rights. Reference herein to any specific commercial product, process, or service by trade name, trademark, manufacturer, or otherwise does not necessarily constitute or imply its endorsement, recommendation, or favoring by the United States Government or any agency thereof. The views and opinions of authors expressed herein do not necessarily state or reflect those of the United States Government or any agency thereof.

Abstract

Measurement and Interpretation of Seismic Velocities and Attenuations in Hydrate-Bearing Sediments

Grant/Cooperative Agreement DE-FE 0009963.

- We formed methane hydrates using the ice seeding method with ice particles of 500 μm in diameter, at a temperature of $-10\text{ }^{\circ}\text{C}$ and pressure of 1500 psi
- Low frequency measurements were performed on an aluminum standard for a frequency sweep of 1 to 2000 Hz while rotating a semiconductor gage through all 12 acquisition channels. We measured a Poisson's Ratio of 0.42 for the aluminum sample.
- We obtained μCT images of clean quartz sand with 40 % and 80 % THF hydrate saturation. The images appear to show pore filling hydrate with partial cementation of the grains
- We performed μCT imaging on a sample consisting of quartz sand with 30 wt% bentonite and 80% THF hydrate saturation. It appears that the clay is moved during the hydrate formation process causing significant heterogeneity in clay content and hydrate saturation.
- Our two submitted manuscripts to Geophysical Prospecting have been returned with comments. They are now being prepared for resubmission.

Table of Contents

Disclaimer	1
Abstract	3
Table of Contents	4
List of Figures and Tables	5
<i>List of Figures</i>	5
<i>List of Tables</i>	5
2. Accomplishments	6
2.1 <i>Overview of Milestone Status</i>	6
2.2 <i>Methane Hydrate Formation</i>	8
2.3 <i>Low Frequency Measurements</i>	9
2.4 <i>μCT Imaging of THF-Hydrate Bearing Clean Quartz Sand and Quartz Sand with Bentonite</i>	15
3. Acknowledgments	20
4. Plans	21
5. Products	22
6. Participants and Collaborating Organizations	23
7. Changes / Problems	26
8. Special Reporting Requirements	27
9. Budgetary Information	28

List of Figures and Tables

List of Figures

Figure 1. Milestone Status. We are at the end of our thirteenth quarter and are approaching the start of the final phase of this project.	6
Figure 2 Methane hydrate	8
Figure 3: Measured strain response of a semiconductor gage which was glued onto aluminum in axial direction (Young's gage)	11
Figure 4: Measured strain response of a semiconductor gage which was glued onto aluminum in axial direction (Young's gage) with a significant noise level below 10 Hz.	12
Figure 5: Measured strain responses of a semiconductor gage which was glued onto aluminum in axial direction (Young's gage) and measured in all of the 12 channels.	12
Figure 6: Calculated Poisson's Ratio from all the channels for aluminum.	13
Figure 7: Strain Measurements for different combinations for the power supply for the Wheatstone bridge.	13
Figure 8: Calculated Poisson's Ratios for different power supply combinations for the Wheatstone bridge.	14
Figure 9: Calculated Poisson's Ratio for 2000 measurements from 20 Hz to 2000 Hz. ...	14
Figure 10: μ CT images showing horizontal and vertical slices through a quartz sand sample a) and b) with $Sh=80\%$. c) and d) at room temperature after dissociation of THF hydrate for comparison. Dark gray areas indicate hydrate, light gray areas represent barium chloride brine in the pore space. Resolution: $7.38\mu m$	15
Figure 11: μ CT images showing horizontal and vertical slices through a quartz sand sample a), b) and c) with $Sh=40\%$. d), e) and f) at room temperature after dissociation of THF hydrate for comparison. Dark gray areas indicate hydrate, light gray areas represent barium chloride brine in the pore space. Resolution: $15.32\mu m$	16
Figure 12: μ CT images showing horizontal and vertical slices through a quartz sand sample with 30 wt% clay (bentonite) a) and b) with $Sh=80\%$. c) and d) at room temperature after dissociation of THF hydrate for comparison. Dark gray areas indicate hydrate, light gray areas represent barium chloride brine and clay minerals. Resolution: $7.38\mu m$	18
Figure 13: μ CT images of quartz sand sample with 30 wt% clay (bentonite) with $Sh=80\%$. A bigger area of the sample is shown here to emphasize the heterogeneity in hydrate distribution. Dark gray areas indicate hydrate, light gray areas represent barium chloride brine and clay minerals, white areas are precipitated barium chloride. Resolution: $20.44\mu m$	19

List of Tables

Table 1. Milestone status	7
Table 2. Q12 Milestones and Deliverables	21

2. Accomplishments

2.1 Overview of Milestone Status

Our current position is shown by a red bar in the Gantt chart in Figure 1. The Milestone status is shown in Table 1. In the current period of Q13 (Q1 of Year 4), we continued our work on Task 9 – MXCT Characterization. We worked on attenuation properties of hydrates forming out of solution (Task 7). This is fundamental work which will be used for Task 11 – Comparison with Log Data.

We requested and got approval for a no-cost extension of the project until April 30, 2016. This extension will allow us to catch up for setbacks in our progress on CH₄ hydrates. A post-doctoral scholar, Dr. Ahmad A. A. Majid has joined the group. Dr. Majid has experience in making CH₄ hydrates and has redesigned his old setup for our experiments. Given our success to make methane hydrates, we anticipate requesting an additional no-cost extension to end of 2016 to be able to make the methane hydrate measurements.

Students: Ms. Mandy Schindler will defend her thesis proposal in the coming quarter (Q14).

Publications: The two manuscripts submitted to Geophysical Prospecting have been returned with comments. They are now being prepared for resubmission.

Cost share: We anticipate covering the MXCT cost share by way of salaries and imaging costs in the next report.

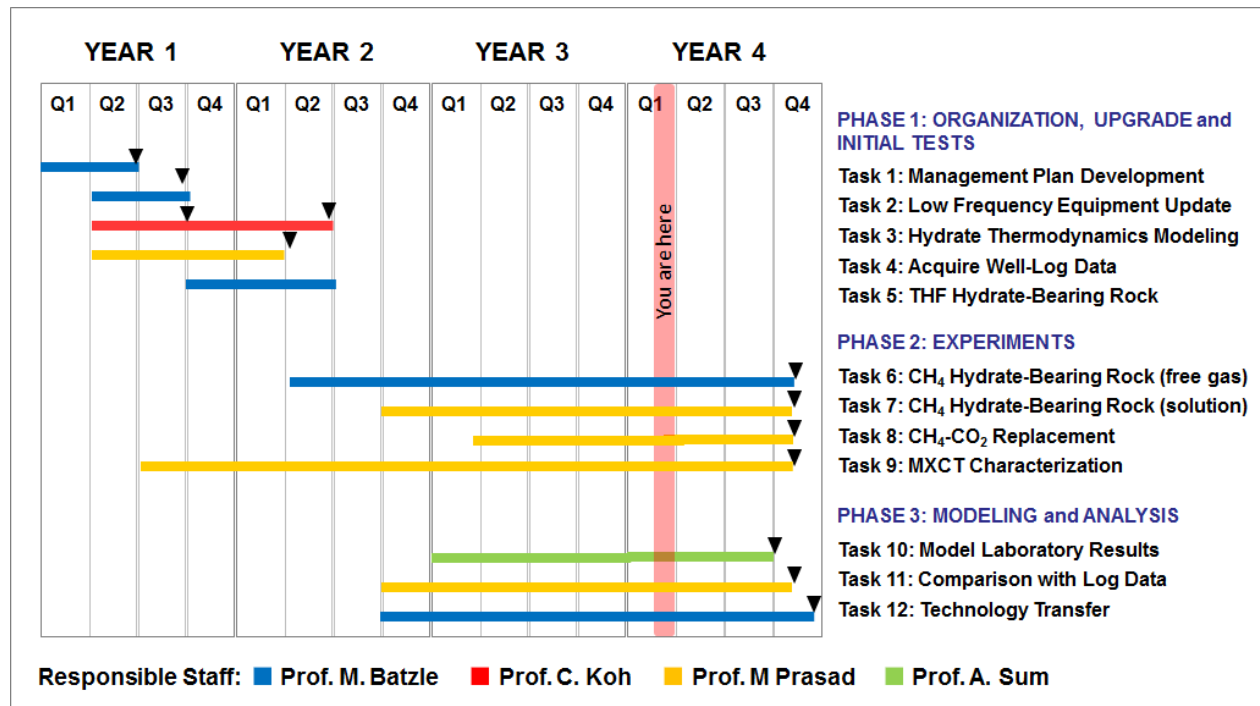


Figure 1. Milestone Status. We are at the end of our thirteenth quarter and are approaching the start of the final phase of this project.

Table 1. Milestone status

Milestone	Title / Description	Status	Completion date (completed or expected)
Completed			
1	Project Management Plan (PMP)	Complete & approved	1 Dec 2012
2	Modifications to low frequency system	Completed	1 June 2013
3	Modeling established using EOS	Completed	31 May 2014
4	Property models of hydrates completed	Completed	31 May 2014
5	Logs acquired and database established	Completed	15 Jun 2014
6	THF hydrate grown in pressure vessel	Completed	15 Apr 2014
7	Methane hydrates from free gas phase (somewhat behind schedule)	Continuing*	31 Dec 2016
Continuing or Planned			
8	Methane hydrates from gas in solution	Planned	31 Dec 2016
9	CO2 replacing methane in hydrates	Planned	30 Sep 2016
10	MXCT scans conducted	Continuing*	30 Sep 2016
11	Effective media models complete	Planned	30 Sep 2016
12	Comparison to in situ data complete	Planned	15 Oct 2016
13	Information Dissemination	Continuing*	31 Dec 2016
*initial stages were completed on schedule, but the process continues throughout the project			

2.2 Methane Hydrate Formation

Experimental Procedure

In this work, methane hydrates were formed by converting ice particles to hydrates at low temperature high pressure. The procedure for methane hydrates formation began by first preparing the ice particles. This was done by crushing ice using an ice crusher at liquid nitrogen temperature. The crushed ice was then sieved to obtain size-controlled ice particles (approximately 500 μm). The ice particles were then added into the pressure cell that has been cooled to $-10\text{ }^{\circ}\text{C}$. The cell has to be decreased to $-10\text{ }^{\circ}\text{C}$ in order to avoid the ice particles from melting. Next, the cell was properly sealed and placed in a cooling bath that has been set at constant temperature of $-10\text{ }^{\circ}\text{C}$. After this step, the cell was slowly pressurized with methane gas until the system pressure reaches a pressure of 1500 psig. At this pressure, the system has a high degree of subcooling (ΔT_{sub}) of $\sim 23\text{ }^{\circ}\text{C}$. It should be noted that in order to avoid hydrate dissociation, the gas that was injected into the cell was pre-cooled before entering the cell. This was done by immersing the gas inlet line in the cooling bath. Finally, the system was left at this condition (1500 psig and $-10\text{ }^{\circ}\text{C}$) for several days for hydrate formation. The analysis of hydrate conversion was determined by performing mass balance; specifically by calculating the mole of methane at the beginning of the test and at the end of test.

Experimental Result

Figure below shows that methane hydrates that was formed using this setup.



Figure 2 Methane hydrate

2.3 Low Frequency Measurements

Over the last couple of months we have been working on the calibration for our updated low-frequency device.

First step of the update involved new wiring and connectors between the computer and the top part of the low frequency device. As reported before, we changed our data acquisition system. This new system enables us to perform our experiments faster and we are able to record more and all of the different channels simultaneously. With this increase in channels, we also changed the wiring within the device and we upgraded our Wheatstone bridge to now being able to support 12 channels at the time.

To calibrate our setup we use aluminum as our standard. We glued semiconductor gages onto the surface of an aluminum rod and glued this rod into our low frequency device. For this test we used semiconductor gages because of the low strain that is applied during our experiment (10^{-6} - 10^{-7}) and aluminum being an extremely stiff material. Semiconductor gages are more sensitive to deformation compared to foil gages.

The first set of experiments consisted of checking each single channel regarding its readings. Therefore we rotated two Poisson's gages and one Young's gage through all of the channels. Figure 3 shows the measured strain data for a frequency sweep from 1 Hz to 2000 Hz for a semiconductor gage which was glued onto aluminum in axial direction, for Channel Two. This measurement shows no significant influence from external noise sources such as power lines. But it is noticeable that at higher frequencies (>100 Hz) the measurement shows some sort of resonance in the data. Figure 4 shows the measured strain response for Channel Five for the same semiconductor gage. In the lower frequencies (1 Hz – 10 Hz) the data is scattered and dominated by noise. Past 10 Hz the recorded data is similar to the one from Channel Two. This becomes more obvious in Figure 5 which shows all of the measured strains for one semiconductor gage for all 12 channels. This set of experiments showed us that two of the channels are not working at all (Channel 3 and 10). Also, two of the channels are significantly influenced by some low frequency noise (Channel 5 and 7) but they could still be used for measurements that are performed above 10 Hz. All of the other eight Channels (1, 2, 4, 6, 8, 9, 11, and 12) measured almost identical strains from 1 Hz to 2000 Hz with the same resonances at higher frequencies. Simultaneously, while rotating an axial semiconductor gage through all of the channels we also measured and rotated a radial semiconductor gage through all of the channels. Having the strain information from both semiconductor gages allows us to directly calculate the Poisson's Ratio which is defined by the radial strain divided by the axial strain (Figure 6). The calculated data shows a very distinct linear trend between 1 Hz and 100 Hz. As we expected, with increasing frequency the Poisson's Ratio keeps constant. This is a key factor in calibrating our device and why we chose aluminum. Aluminum does not attenuate or disperse the signal. After that frequency the previously mentioned resonance influences the Poisson's Ratio. The calculated Poisson's Ratio (0.42) is within its physical limits (0 – 0.5) but is significantly higher than the specified Poisson's Ratio (0.35) for the specific type of aluminum used.

We are now investigating the reasons for the mismatch in Poisson's Ratio from the literature. One potential source of error is the power source for the Wheatstone bridge. Our experiments are conducted with a 12 V car battery as voltage source for the Wheatstone bridge. We tested this hypothesis by first connecting the battery to a power supply box that was then adjusted to supply a constant 12 Volts. In the second test, the car battery was connected directly to the Wheatstone bridge. An additional test was made with a new car battery connected directly to the Wheatstone

bridge. And finally, the new car battery was connected to battery maintainer. The measured strains for each of the four test scenarios can be seen in Figure 7. We observed a drop in amplitude when we compared the data of the old car battery + power supply with just the old car battery. We found out that the old battery was not supplying 12 volts anymore and we decided to use a new battery. A constant and known input voltage is necessary to correctly calculate the Young's Modulus. The new battery provided a constant 12 volts. When we connected a battery maintainer, the shape of the measured strain data changed completely. Even though a known voltage is necessary for the Young's Modulus, it is not needed to calculate the Poisson's Ratio. Figure 8 shows the resulting Poisson's Ratios for the four different power supply cases. The battery maintainer influences our measurement strongly resulting in Poisson's Ratio above 0.5 which is implausible. The measurement with the power supply shows that it influences the measurement. The old and new car battery show almost no sign of any noise in the lower frequency range (<100 Hz). Also, even though the old car battery was not providing 12 volts, the Poisson's Ratio is not affected by that, but the Young's modulus would be.

We performed one more experiment to look at the higher frequencies and the observed resonance. Figure 9 shows a frequency sweep from 20 Hz to 2000 Hz with 2000 measurement points. Now, the frequency of the power lines shows up in our data at 60 Hz and one of its multiples at 180 Hz which causes the data to randomly spread. Also, the resonance for example at around 100 Hz is smooth and so are all the other resonances. Usually when we measured samples with our low frequency apparatus these resonances occurred around or past 2000 Hz. We observe this shift in resonance due to the stiffness of the aluminum.

To continue the calibration for the low frequency device we plan on measuring a softer standard, PEEK. To test this kind of material with our low frequency device we are also preparing ultrasonic transducers made from aluminum. We hope to finish the calibration within the first half of the next quarter.

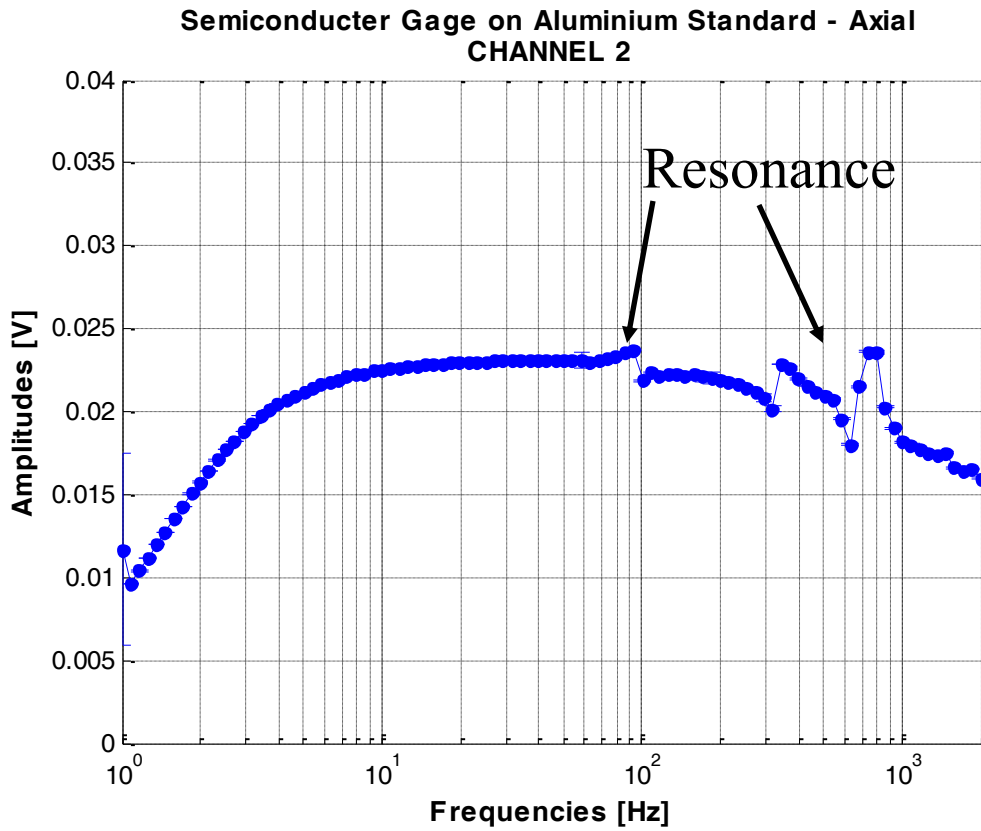


Figure 3: Measured strain response of a semiconductor gage which was glued onto aluminum in axial direction (Young's gage)

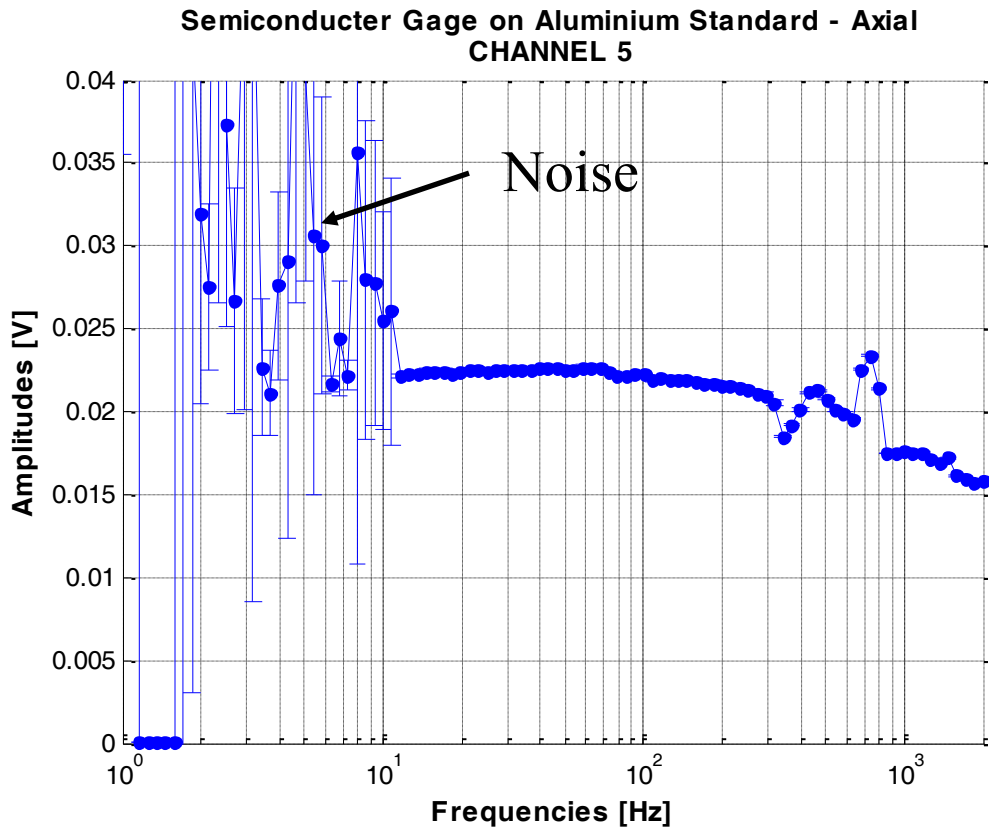


Figure 4: Measured strain response of a semiconductor gage which was glued onto aluminum in axial direction (Young's gage) with a significant noise level below 10 Hz.

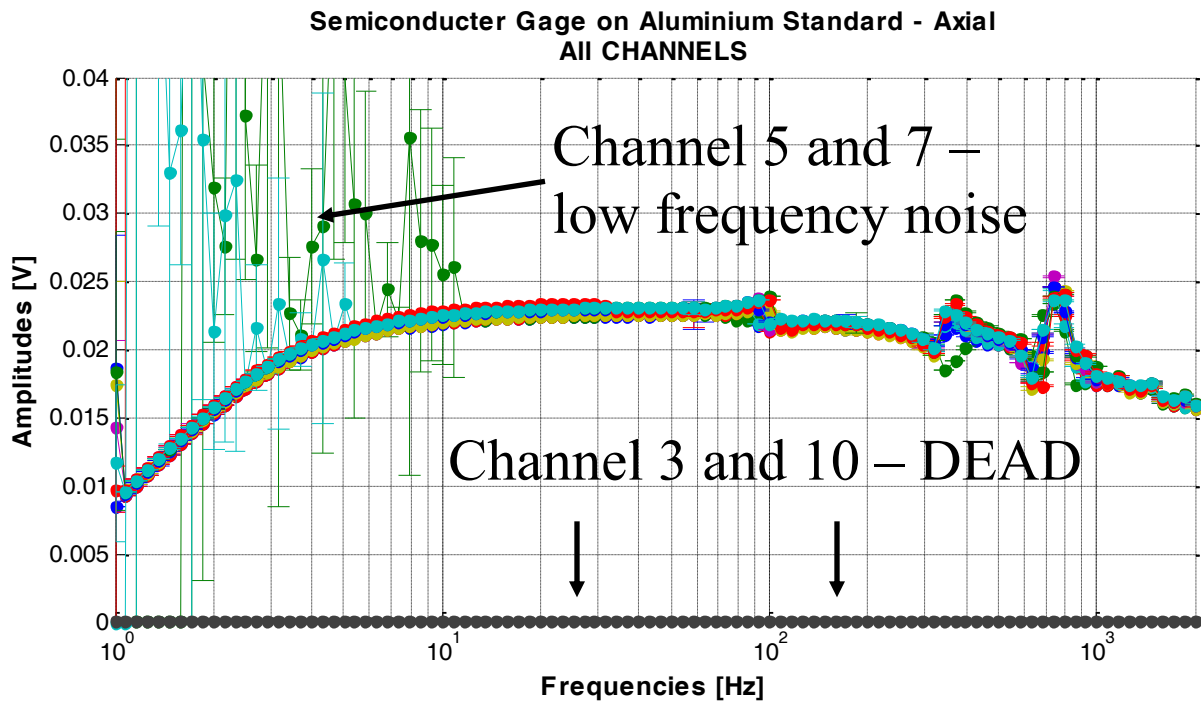


Figure 5: Measured strain responses of a semiconductor gage which was glued onto aluminum in axial direction (Young's gage) and measured in all of the 12 channels.

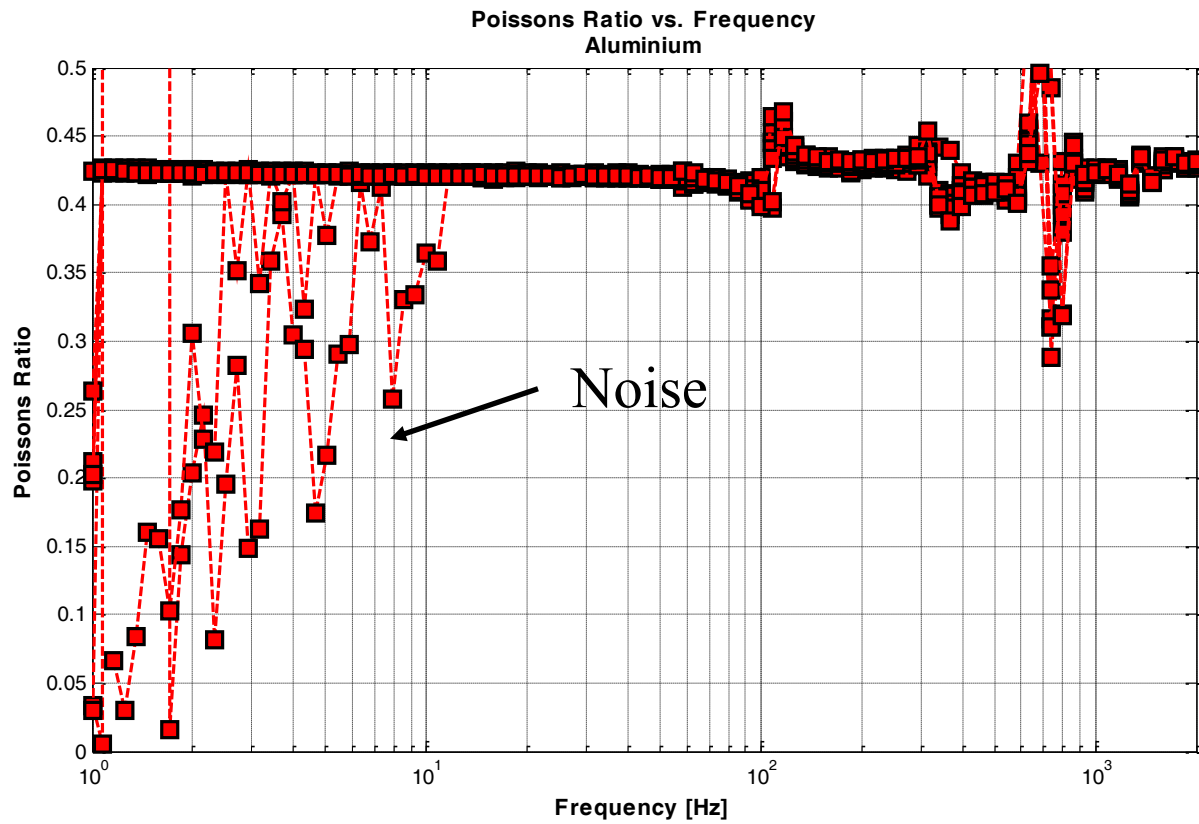


Figure 6: Calculated Poisson's Ratio from all the channels for aluminium.

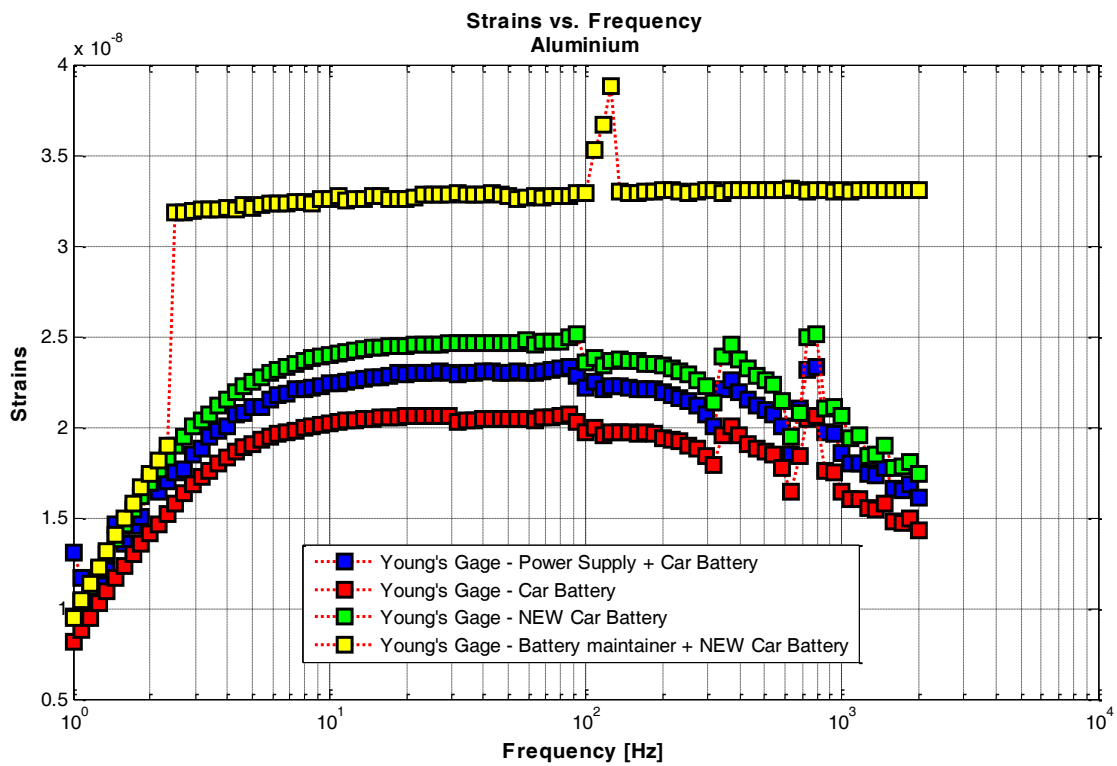


Figure 7: Strain Measurements for different combinations for the power supply for the Wheatstone bridge.

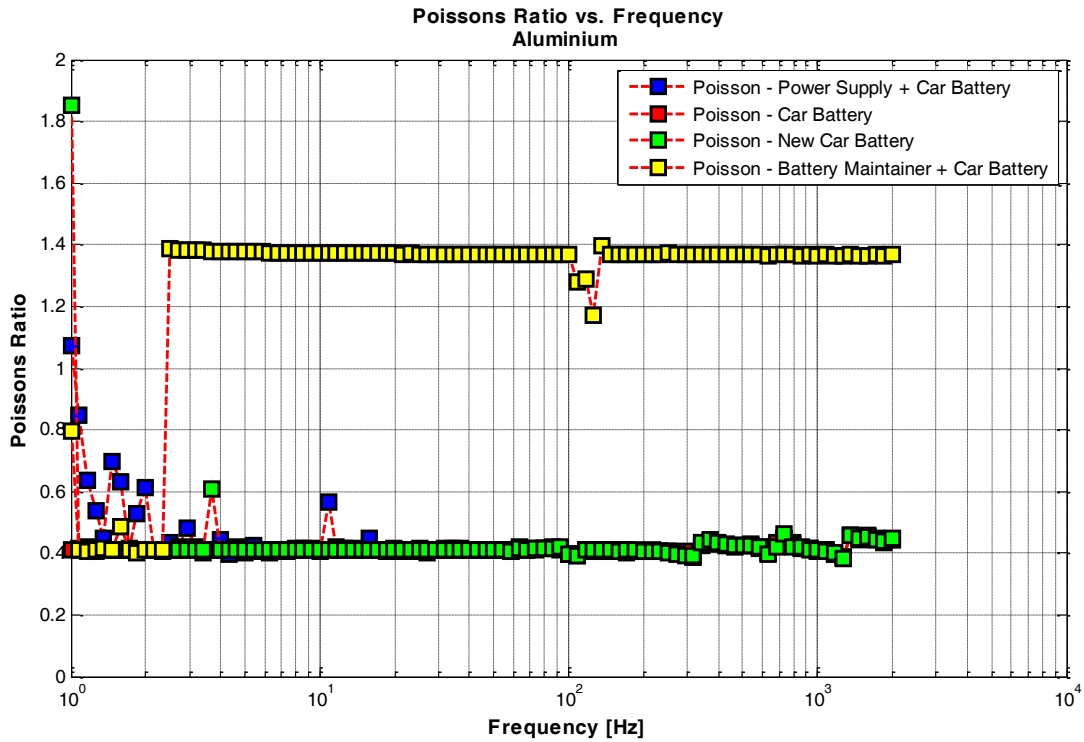


Figure 8: Calculated Poisson's Ratios for different power supply combinations for the Wheatstone bridge.

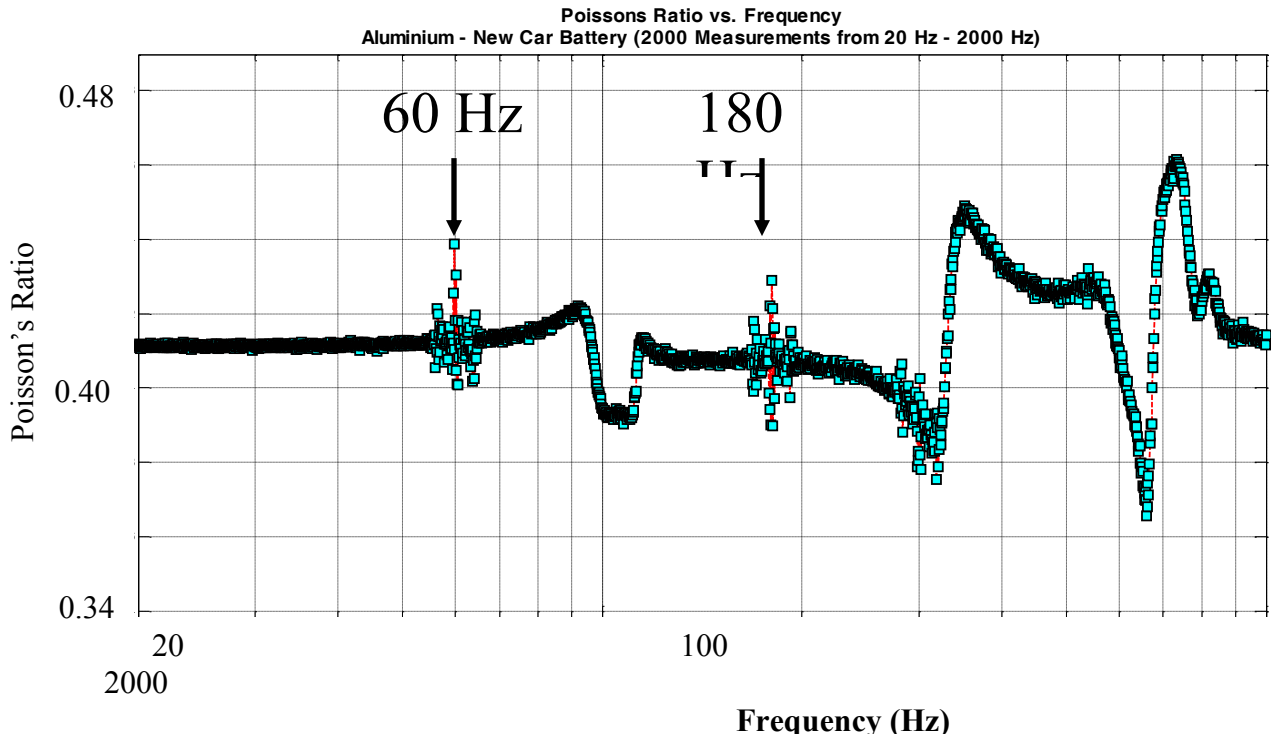


Figure 9: Calculated Poisson's Ratio for 2000 measurements from 20 Hz to 2000 Hz.

2.4 μ CT Imaging of THF-Hydrate Bearing Clean Quartz Sand and Quartz Sand with Bentonite

The made μ CT images of THF-Hydrate Bearing Clean Quartz Sand and Quartz Sand with Bentonite. The reconstructed μ CT images (Figure 10 and Figure 11) contain information about the distribution of different components in the sample. Different gray values in the CT images represent different X-ray attenuation values in the sample. Because of its low attenuation THF hydrate has low gray-values and appears as dark gray areas in the μ CT images whereas barium chloride brine has higher gray values caused by its higher attenuation value and is displayed in light gray. The black areas in the pore space represent trapped air bubbles.

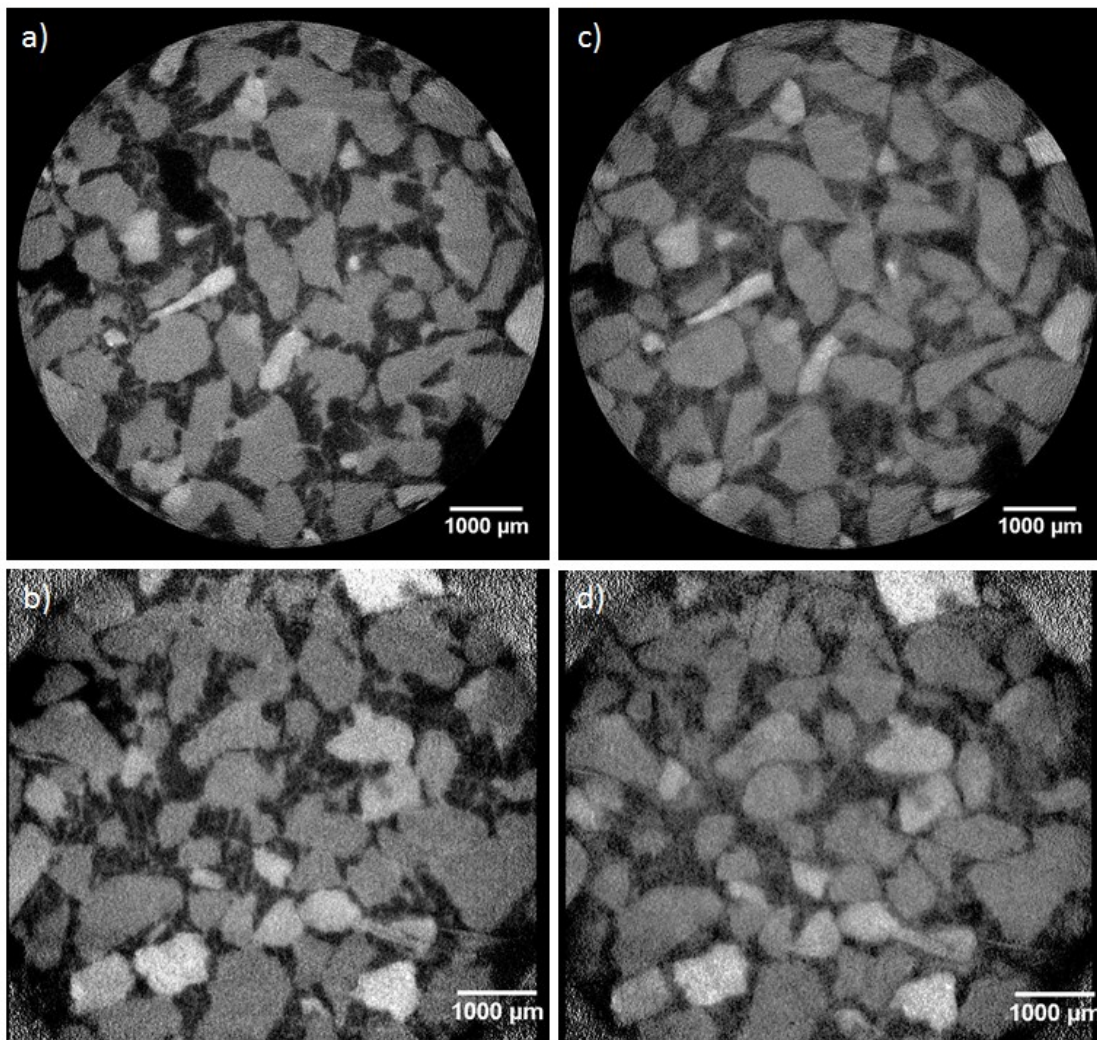


Figure 10: μ CT images showing horizontal and vertical slices through a quartz sand sample a) and b) with $Sh=80\%$. c) and d) at room temperature after dissociation of THF hydrate for comparison. Dark gray areas indicate hydrate, light gray areas represent barium chloride brine in the pore space. Resolution: $7.38\mu m$

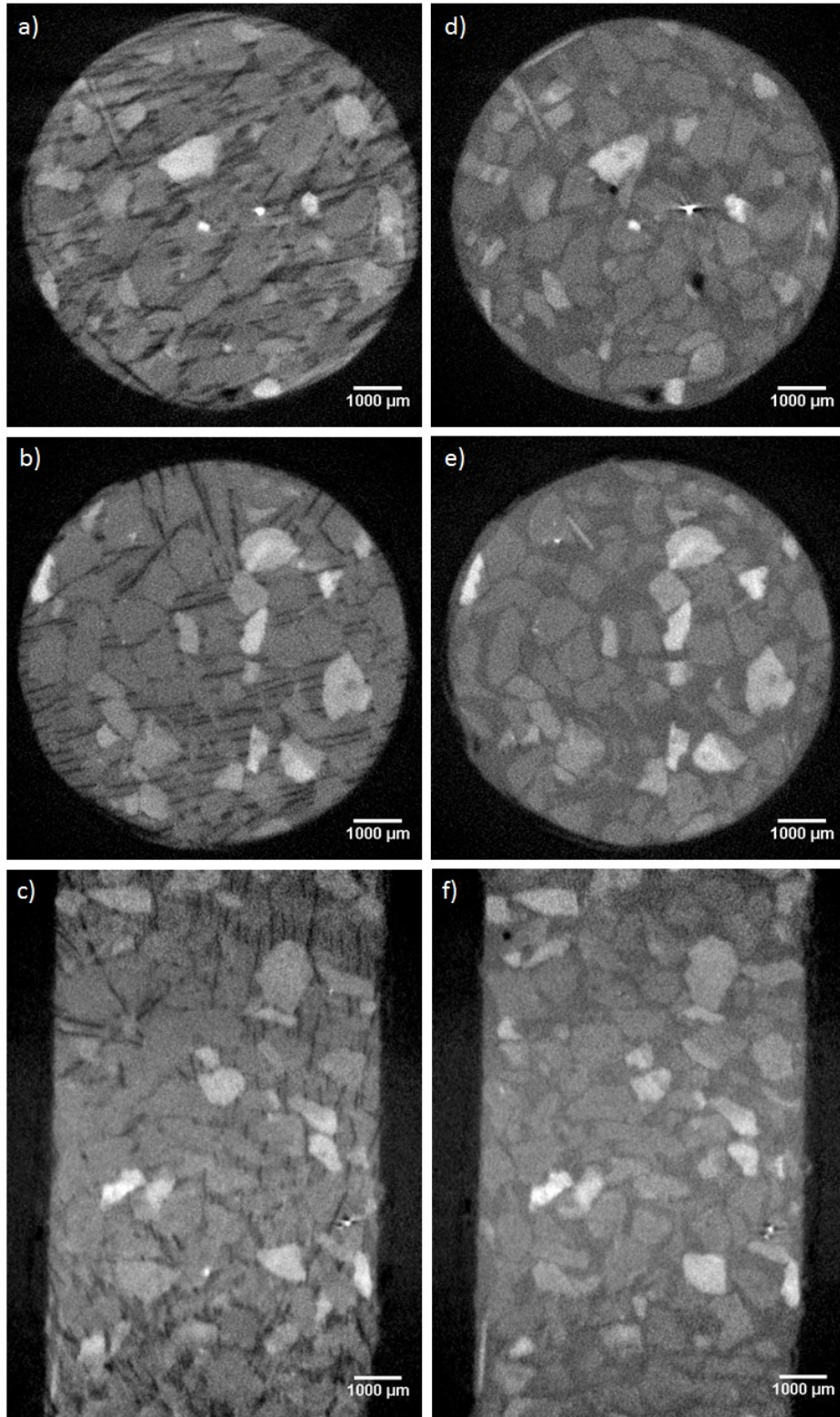


Figure 11: μ CT images showing horizontal and vertical slices through a quartz sand sample a), b) and c) with $Sh=40\%$. d), e) and f) at room temperature after dissociation of THF hydrate for comparison. Dark gray areas indicate hydrate, light gray areas represent barium chloride brine in the pore space. Resolution: $15.32 \mu\text{m}$

Figure 10 shows CT images for a sample with 80% hydrate saturation and the same areas of the sample at room temperature without hydrate. The images indicate that THF hydrate is located in the pore body and is interrupted by randomly shaped areas filled with barium chloride brine. The barium chloride brine appears to cover the surfaces in some areas (indicated by light gray layer on grain surface and rougher, more irregular surfaces in Figure 10a and Figure 10b but not in Figure 10c and Figure 10d). Some small pores are entirely filled with barium chloride brine. Hydrate saturation and distribution appears homogeneous in this sample. The distribution pattern indicates that hydrate starts to grow in the pore bodies and grows towards the grains resulting in embedded areas of barium chloride brine and a layer of barium chloride brine on some of the grain surfaces. The resolution of $7.38\ \mu\text{m}$ poses a limit for the interpretation of our images: the THF hydrate appears to touch the grain surfaces in some areas, however, it cannot be ruled out that there is a micro layer of barium chloride brine between the grain and the hydrate which is not resolved in our images. Such micro layers have been described by Sell et al. (2015). Due to the higher resolution of their images (200 nm) they observed a micro layer of water between quartz grain surfaces and xenon hydrate layers.

Figure 11 shows a sample with 40% hydrate saturation (Images a,b and c) and at room temperature without hydrate in the pore space (images d, e and f). The hydrate distribution differs significantly from the one observed at 80% hydrate saturation (Figure 10). Note that this sample needed to be cooled to around $-1\ ^\circ\text{C}$ and it is thus possible that ice was formed in addition to hydrate. Images 11a and c show slices from the bottom of the sample and Images 11b and d are slices near the top of the sample. We observed a more heterogeneous distribution of hydrate. The saturation seemed to vary from top to bottom of the sample and the pattern changed from a mixing of barium chloride brine (or ice) and hydrate (Figure 11a) to discrete needle shaped inclusions of hydrate in a mainly barium chloride brine filled pore space (Figure 11b). The heterogeneity could be explained by a temperature gradient from top to bottom of the sample caused by the cooling system. The difference in hydrate distribution compared to the 80% sample indicate that the same formation method may result in different hydrate distributions and can differ from the distribution models used for effective medium modeling. Although hydrate is located in the bulk pore volume, it seems to contact the grain surfaces as well and thus cement the sediment. That means the hydrate is not strictly confirming one distribution model (the pore filling model). A mixing of hydrate suspended in the pore fluid with hydrate partially cementing the grains is possible. This behavior has been described by Fabricius (2003) as IF (isoframe) models.

Figure 12 shows a sample that contains a mixture of quartz grains and bentonite (30 wt%) as host sediment. A THF-water-BaCl₂ mixture which yields 80% hydrate saturation was added. Figure 12 locally shows a similar hydrate distribution pattern as the clay free sample with 80% hydrate saturation: hydrate is located in the pore bodies, barium chloride brine covers surfaces and grows in needle-like random shapes into the pore space. The white streaks in Figure 13 show pure barium chloride which was precipitated when water molecules from the barium chloride brine were absorbed by clay minerals. When considering a bigger area of the sample (Figure 13) I observed a more pronounced heterogeneity. The left side in Figure 13a and the upper

part of Figure 13b clearly show higher hydrate saturations than the right and lower part, respectively. This observation indicates that clay in the pore space is moved during hydrate formation and accumulates in some areas of the sample while other pores are deprived of clay and are almost entirely filled with hydrate. However, the clay-filled pores still seem to bear hydrate intermixed with the clays (see for example at the bottom of Figure 12a). This behavior leads to significant heterogeneity which violate the assumptions of the effective medium approach. A more complex model is required to explain changes in elastic properties caused by hydrate-clay distribution observed in this sample. The μ CT images show that hydrate forms in the pores as part of the pore fluid and as cement. The presence of clay causes more heterogeneity in hydrate distribution and a mixing of hydrate and clay in the pore space. Given that THF hydrate is a proxy for one possible texture of natural occurring hydrate, we conclude that natural gas hydrate in coarse grained sediments is partially suspended in the pore fluid and partially load bearing when formed from natural gas dissolved in water. This conclusion is essential for the assessment of gas hydrate saturation from seismic and well log data

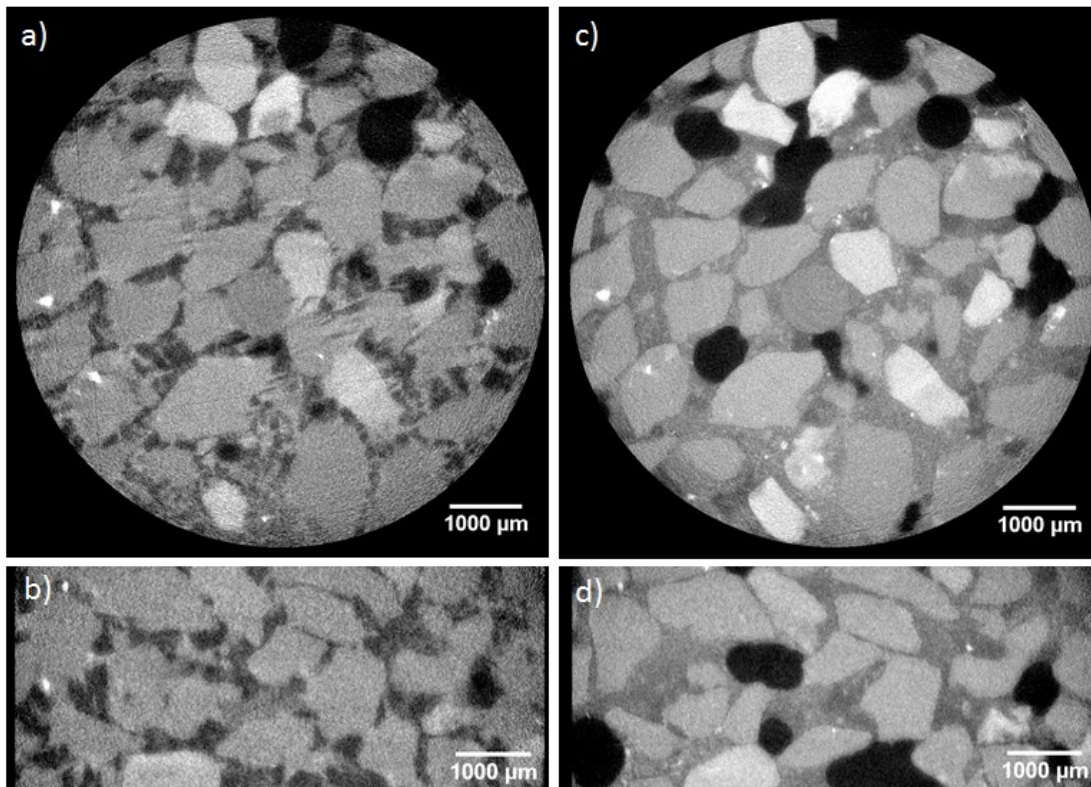


Figure 12: μ CT images showing horizontal and vertical slices through a quartz sand sample with 30 wt% clay (bentonite) a) and b) with $S_h=80\%$. c) and d) at room temperature after dissociation of THF hydrate for comparison. Dark gray areas indicate hydrate, light gray areas represent barium chloride brine and clay minerals. Resolution: 7.38 μ m

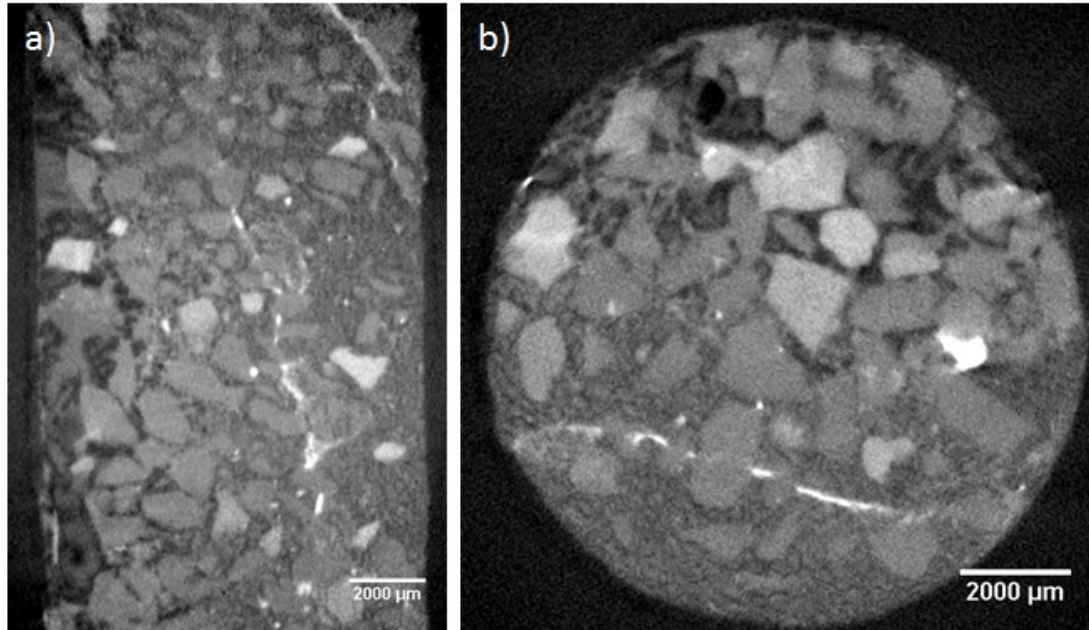


Figure 13: μ CT images of quartz sand sample with 30 wt% clay (bentonite) with $Sh=80\%$. A bigger area of the sample is shown here to emphasize the heterogeneity in hydrate distribution. Dark gray areas indicate hydrate, light gray areas represent barium chloride brine and clay minerals, white areas are precipitated barium chloride. Resolution: 20.44 μ m

References

Fabricius, I. L. 2003. How burial diagenesis of chalk sediments controls sonic velocity and porosity. *AAPG Bulletin*, 87(11), 1755{1778}.

Sell, K., Chaouachi, M. and Falenty, A., Saenger, E. H., Khan, F. and Schwarz, J.-O., Enzmann, F., Kersten M., and Kuhs, W. F. 2015. Microstructure of hydrate-bearing sediments and determination of P-wave velocities based on high-resolution synchrotron tomographic data. In: *Proceedings of the SEG annual meeting*, October 2015, New Orleans.

3. Acknowledgments

We thank the US Department of Energy for sponsoring the project. We also thank Tim Collett for his cooperation with us on this project. We acknowledge support of some personnel by other grants (DHI/Fluids and OCLASSH consortia, Chinese Mining University).

4. Plans

We plan to focus on CH₄ hydrates in acoustics, low frequency measurements and MXCT scanning. For that purpose we will collaborate with the Center for Hydrate Research in the Department of Chemical Engineering at Colorado School of Mines to make use of their expertise with methane hydrates. We will continue our work on NMR measurements of hydrate-bearing sediments and work on a cooling system for the NMR machine. The newly developed ability to obtain ultrasonic data during MXCT imaging will be applied to hydrate-bearing sediments.

Table 2. Q12 Milestones and Deliverables

Milestone	Task	Description	Anticipated Completion date	Report Content
7	6	Methane hydrates from free gas phase	12/31/2016	Progress report
10	9	NMR/MXCT characterization	9/30/2016	Progress report
12	11	Comparison to log data	12/31/2016	Progress report
13	12	Information dissemination via publications, student theses, and conferences	12/31/2016	Progress report

5. Products

Publications (Publications; Conference Papers, Presentations, Books)

Pohl, M., Prasad, M., Batzle†, M. L., Ultrasonic Attenuation of Pure THF-Hydrate:
Geophys. Prosp. (submitted).

Schindler, M., Batzle†, M. L., Prasad, M., Micro X-Ray Computed Tomography
Imaging and Ultrasonic Velocity Measurements in Hydrate-Bearing Sediments:
Geophys. Prosp. (submitted).

Website or other Internet sites

<http://crusher.mines.edu/CRA-DOE-Hydrates>

Technologies or techniques

Nothing to report

Inventions, patent applications and/or licenses

Nothing to report

Other Products

Nothing to report

6. Participants and Collaborating Organizations

CSM personnel:

Name:	Manika Prasad
Project Role:	Principle Investigator
Nearest person month worked this period:	0.25
Contribution to Project:	Dr. Prasad helped with acoustic and attenuation measurements
Additional Funding Support:	Academic faculty
Collaborated with individual in foreign country:	No
Country(ies) of foreign collaborator:	N/A
Travelled to foreign country:	Yes
If traveled to foreign country(ies),	India, Singapore, Germany
Duration of stay:	3 weeks

Name:	Michael Batzle†
Project Role:	
Nearest person month worked this period:	0
Contribution to Project:	Dr. Batzle was responsible for the overall (dis)organization of the project.
Additional Funding Support:	Academic faculty
Collaborated with individual in foreign country:	No
Country(ies) of foreign collaborator:	N/A
Travelled to foreign country:	No
If traveled to foreign country(ies),	N/A
Duration of stay:	N/A

Name:	Carolyn Koh
Project Role:	Co- Investigator
Nearest person month worked this period:	0.25
Contribution to Project:	Dr. Koh helped with CH ₄ hydrate experimental setup and measurements
Additional Funding Support:	Academic faculty
Collaborated with individual in foreign country:	No
Country(ies) of foreign collaborator:	N/A
Travelled to foreign country:	No
If traveled to foreign country(ies),	N/A
Duration of stay:	N/A

Name:	Weiping Wang
Project Role:	Laboratory Manager

Nearest person month worked this period:	1
Contribution to Project:	Mr. Wang assisted in equipment fabrication
Additional Funding Support:	DHI/Fluids consortium, Chinese Mining University
Collaborated with individual in foreign country:	No
Country(ies) of foreign collaborator:	N/A
Travelled to foreign country:	Yes
If traveled to foreign country(ies):	China
duration of stay: N/A:	2 weeks

Name:	Mathias Pohl
Project Role:	Ph.D. student
Nearest person month worked this period:	3
Contribution to Project:	Mr. Pohl prepared samples and collected ultrasonic data.
Additional Funding Support:	N/A
Collaborated with individual in foreign country:	N/A
Country(ies) of foreign collaborator:	N/A
Travelled to foreign country:	Yes
If traveled to foreign country(ies)	Germany, Spain, Ireland
duration of stay:	3 weeks

Name:	Mandy Schindler
Project Role:	Ph.D. student
Nearest person month worked this period:	3
Contribution to Project:	Ms. Schindler prepared samples and collected CT data.
Additional Funding Support:	N/A
Collaborated with individual in foreign country:	No
Country(ies) of foreign collaborator:	N/A
Travelled to foreign country:	Yes
If traveled to foreign country(ies),	Germany
duration of stay:	2 weeks

Name:	Ahmad Afif Abdul Majid
Project Role:	Post Doctoral Scholar
Nearest person month worked:	1
Contribution to Project:	Dr. Majid helped setting up our experiment to form methane hydrates out of free gas
Additional Funding Support:	Center for Hydrate Research
Collaborated with individual in foreign country:	No
Country(ies) of foreign collaborator:	N/A
Travelled to foreign country:	No

If traveled to foreign country(ies):	N/A
duration of stay:	N/A

External Collaborations:

Dr. Tim Collett
US Geologic Survey
Denver, Colorado

Support: Dr. Collett provided data and guidance on interpretation and application. He continues to publish numerous papers on hydrate properties.

7. Changes / Problems

1. We requested and got approval for a no-cost extension of the project until April 20, 2016. This extension will allow us to catch up for setbacks in our progress on CH₄ hydrates.
2. Given our late success in making the methane hydrates, we anticipate requesting an additional no-cost extension until 12/31/2016. This will allow us to make methane hydrates with simultaneous acoustic and NMR measurements as well as MXCT imaging.
3. A post-doctoral scholar, Dr. Ahmad A.A.Majid has joined the group. Dr. Majid has experience in making CH₄ hydrates and has redesigned his old setup for our experiments.
4. Once CH₄ hydrates have been successfully formed in sediments, we will use the same setup to replace methane hydrates with CO₂ hydrates

8. Special Reporting Requirements

None

9. Budgetary Information

Attached separately